International Journal of Nanomedicine

Dovepress
open access to scientific and medical research

Open Access Full Text Article

ORIGINAL RESEARCH

A Combinatorial Approach for the Fabrication of Magneto-Optical Hybrid Nanoparticles

This article was published in the following Dove Press journal:
International Journal of Nanomedicine

Dmitry S Koktysh[1,2]
Wellington Pham[3–5]

[1]Department of Chemistry, Vanderbilt University, Nashville, TN 37235, USA; [2]Vanderbilt Institute for Nanoscale Science and Engineering, Vanderbilt University, Nashville, TN 37235, USA; [3]Institute of Imaging Science, Vanderbilt University, Nashville, TN 37232, USA; [4]Department of Radiology and Radiological Sciences, Vanderbilt University, Nashville, TN 37232, USA; [5]Department of Biomedical Engineering, Vanderbilt University, Nashville, TN 37235, USA

Introduction: The increasing demands for better resolution combined with anatomical information in biomedical imaging necessitate the development of multimodal contrast agents. In this respect, the multivalency of nanotechnology enables the integration of nanomaterials with distinct biophysical properties into a unique probe, capable to exert superior imaging characterstics through synergistic enhancement unmatched by any single modality.

Materials and methods: Novel magneto-optical hybrid nanoparticles (MOHNPs), comprise semiconductor quantum dots (QDs) tethered on the surface of superparamagnetic iron oxide (SPIO) NPs, were synthesized using a combinatorial approach. The semiconductor components utilized for the synthesis of the hybrid NPs contained cadmium-free QDs, which were stabilized by a variety of functional ligands including thiols, polyethyleneimine (PEI) and amphiphilic polymers. While SPIO NPs were further modified with silica or PEI on the outermost layer. The main mechanism to assemble semiconductor QDs onto the SPIO NPs employed a core-shell approach, in which covalent bonding and electrostatic interaction held the components together.

Results: The versatility of the NP assembling mechanism described in this work offered a robust and flexible fabrication of MOHNPs. A proof-of-concept study demonstrated desterous coating of folic acid onto the surface of MOHNPs to create a targeted imaging probe. The emission of the resulted hybrid NPs extended in the near-infrared region, suitable for in vivo applications.

Conclusion: This novel assembling technology offers far-reaching capabilities to generate complex multimodal nanoiamging probes.

Keywords: magnetic nanoparticles, quantum dots, imaging agents, hybrid nanoparticles

Introduction

The current development of nanomaterials for biomedical imaging has a penchant toward the construction of multimodal probes for in vivo applications. In particular, hybrid NPs with a combination of magnetic and fluorescence properties leverage the synergy of magnetic resonance imaging (MRI) and optical imaging, respectively.[1–8] Among the fluorescent-emitting optical components, none comes close to what small QDs can offer given their high photostability, broad excitation spectra and narrowly tuned emission spectra; they are ideal candidates for both in vitro and in vivo optical imaging.[9–11] The optical property of QDs can be fine-tuned by modifications of the structure and size to offer a broad optical fluorescence ranging from ultraviolet (UV) to near-infrared (NIR) regions. Further, the large Stokes shift of QDs combined with its unique optical profile enable QDs to be

Correspondence: Dmitry S Koktysh
Department of Chemistry, Vanderbilt Institute of Nanoscale Science and Engineering, Vanderbilt University Station B 351822, Nashville, TN 37235-1822, USA
Tel +1615 343-6763
Email dmitry.koktysh@vanderbilt.edu

Wellington Pham
Institute of Imaging Science, Vanderbilt University School of Medicine, 1161, 21st Avenue South, Nashville, TN 37232-2310, USA
Tel +1615 936-7621
Email wellington.pham@vumc.org

submit your manuscript | www.dovepress.com
DovePress
http://doi.org/10.2147/IJN.S228962

excited with a single wavelength for many corresponding emission spectra, suitable for imaging multiple targets simultaneously.

Meanwhile, the Food and Drug Administration (FDA)-approved superparamagnetic iron oxide (SPIO) nanoparticles (NPs) are now widely used as a contrast agent for clinical MRI.[12–14] The integration of these two distinct types of NPs into a hybrid system will eventually provide powerful imaging data, greater than any single imaging modality.

Currently, assembling of different types of NPs into a hybrid system is achieved by using either a host matrix method or a core-shell approach, in which one type of NP, usually larger material, is coated with the smaller counterparts on the surface.[7,15–17] The main challenge associated with such a nanohybrid design is how to generate a robust fabrication procedure, in which conditions for hybrid NP formulations must be carefully selected so that functional properties of the involved NPs remain unchanged.[7,8] Another challenge in the design involves solubility issue.[2,18] The choice of water-compatible biomaterials is crucial in this operation, particularly; enhanced water-soluble hybrid NPs contributes to successful in vivo applications. Furthermore, the preservation of the chemical and physical stability of the fabricated hybrid NPs is also critical for various suggested applications.[7]

While SPIO NPs are known to be nontoxic, the safety issues QDs nevertheless remain to be seen. Despite their appealing optical properties, such as brightness and tunable luminescence and photostability, the intrinsic toxicity of some of the components, particularly Cd, is an obstacle for the translation into vivo applications. In the recent past, several Cd- and Pb-free alternative materials have been proposed including III-V semiconductor QDs (e.g., InP) and transition-metal doped ZnSe NC.[19,20] Each of these systems offers advantages and disadvantages regarding tunability and purity of the emission wavelength, fluorescence quantum yield (QY), lifetime and photostability. Among the available materials, it seems I-III-VI_2-type semiconductors QDs can serve as an alternative as well. For example, $AgInS_2$/ZnS or $CuInS_2$/ZnS core/shell QDs do not contain any Class A elements (Cd, Pb, and Hg) or Class B elements (Se and As) which lead to much less toxicity and their luminescence can be tuned across a wide range of wavelengths.[20] Particularly, for in vivo imaging and/or ex vivo tissue labeling, absorption and emission of the QDs within the near-infrared (NIR) spectral window of 700–900 nm is desirable given the minimization of light absorption and scattering by molecules present in biological systems, such as water, hemoglobin and oxyhemoglobin, etc.

The development of the MOHNPs described in this work involves the fabrication of nanocomposites from SPIO NPs and cadmium-free semiconductor QDs employing a core-shell approach. The optical properties of the resultant imaging probe can be easily tuned by varying the size and structure of the assembled shell QDs from visible to NIR region.

Materials and Methods

Materials

Ferric chloride hexahydrate (99%), ferrous chloride tetrahydrate (99%), dextran (DX) (M.w. 20,000), zinc chloride (99%), silver nitrate (99.8%), oleylamine (OLA) (70%), benzyl ether (98%), octylphenyl-polyethylene glycol (IGEPAL CA-630), poly(isobutylene-alt-maleic andydride) (PBMA) were purchased from Sigma-Aldrich. Glutathione (GSH) (98%), tetramethylammonium hydroxide (TMAH) (25% solution in methanol), iron(III) acetylacetonate (99%), myristic acid (MA) (99.5%) were purchased from Acros Organics; sodium diethyldithiocarbamate (98%), indium acetate (99.99%), polyethyleneimine (PEI) (99%, M.w. 10,000), zinc acetate (99.98%), copper(I) iodide (99.998%), tetraethylorthosilicate (TEOS) (99%), 3-mercaptopropyltrimethoxysilane (MPTMS) (97%), 1-dodecanethiol (DDT) (98%), dodecylamine (DDA) (98%) were purchased from Alfa Aesar, 3-glycidyloxypropyl-trimethoxysilane (GOPTS) (95%) was from TCI America. All chemical and organic solvents were obtained commercially as analytical-graded materials without further purification.

Synthesis of QDs and SPIO Nanoparticles

$AgInS_2$/ZnS QDs were synthesized according to procedures outlined in the previous work,[21,22] albeit with the following modifications. First, single source precursors $(AgIn)(S_2CN(C_2H_5)_2)_4$ and $Zn(S_2CN(C_2H_5)_2)_2$ were synthesized from respective metal salts and sodium diethyldithiocarbamate. In a typical experiment, an excess amount of $Na(S_2CN(C_2H_5)2$ (3.2 mmol, 4 eq.) in water (10 mL) was added dropwise to a mixture of $In(CH_3COO)_3$ (0.8 mmol, 1eq.) and $AgNO_3$ (0.8 mmol, 1eq.) in DI water (30 mL). One hour after vigorous stirring, the desired product was precipitated and collected by centrifugation (4500 rpm, 10 min) and washed with ddH_2O 3 times and dried under vacuum to provide a teal colored powder. $Zn(S_2CN(C_2H_5)_2)_2$ was synthesized in the same

manner using 0.8 mmol of $ZnCl_2$ and 1.6 mmol of $Na(S_2CN(C_2H_5)_2)$.

$AgInS_2$ (AIS) QDs were synthesized by dispersing the precursor $AgIn(S_2CN(C_2H_5)_2)_4$ (50mg, 0.6 mmol) in 3 mL of OLA solution. The mixture was degassed at 40°C for 30 min followed by quick raise in temperature to 180°C over the course of 5 min under a stream of argon and held at this point to grow the QDs. After 8 min, the brown solution of fabricated QDs was removed by a syringe. After cooling down to room temperature the solution was centrifuged (4500 rpm for 10 min) to remove large agglomerates. AIS QDs in a clear supernatant were further washed from unreacted reagents by centrifugation using acetone (10 mL) to flocculate QDs.

To grow an outer ZnS shell, the AIS QDs were dissolved in a solution of OLA (3.0 mL) containing $Zn(S_2CN(C_2H_5)_2)_2$ (5.0 mmol). The mixture was vacuumed at 120°C for 30 min. Then the temperature was raised to 180°C and set for 20 min. At this point, the synthesized $AgInS_2$/ZnS QDs were washed using the same procedure as for the AIS QDs. Finally, AIS/ZnS QDs were dissolved in chloroform (1.0 mL) before phase-transfer back to aqueous condition by a ligand exchange with GSH using a known procedure.[23–25]

PEI-coated AIS/ZnS QDs were fabricated using previously reported procedure,[26] in which a solution of PEI in chloroform (0.01g/mL) was added dropwise to a mixture of AIS/ZnS QDs in chloroform under vigorous stirring followed by a brief sonication (5min). Two hours later, at the completion of the reaction, chloroform was removed under vacuum, then water (1.0 mL) was added to the reaction flask, and the mixture was vortexed and centrifuged to provide the desired QDs in the supernatant. The extracted QDs were washed with acetone to remove unbound PEI and redispersed in water at a concentration of 0.06 mmol/mL.

$CuInS_2$/ZnS (CIS/ZnS) QDs were synthesized based on a modified protocol[27] where the degassed Cu-thiol stock solution was prepared by dissolving CuI (0.3 mmol) in dodecanethiol (3.0 mL) under argon. One third of that solution was injected into a stirring degassed mixture of $(In(OAc)_3$ (0.1 mmol), MA (0.3 mmol) in ODE (8.0 mL) at 250°C under a stream of argon and QDs were grown at 210°C for 2h. The ZnS shell was deposited by adding $Zn(OAc)_2$ (0.5 mmol) into the reaction solution, which was annealed for 2h at 230°C. At the conclusion of the reaction, CIS/ZnS QDs were phase transferred to water using an amphiphilic polymer according to a reported procedure.[28]

The dextran-coated SPIO NPs were synthesized using the previously reported protocol based on the conversion of ferrous and ferric iron salts at alkaline pH with dextran coating.[25,29,30]

OLA-stabilized Fe_3O_4 NPs were synthesized according to a reported protocol.[31] Briefly, iron(III) acetylacetonate (0.5 mmol) was dissolved in a solution of OLA in benzyl ether (2.5 mL each) followed by heating under vacuum at 110°C for 1h. Then the solution was rapidly heated to 300°C while being purged by argon allowed to remain at this temperature for 1h. At the conclusion of the reaction, the solution was cooled down to room temperature and Fe_3O_4 NPs were purified by acetone and finally redispersed in chloroform. The phase transfer and PEI coating of magnetic NPs were achieved using the procedure noted above for AIS/ZnS QDs.

Synthesis of QD-Laden SPIO Nanoparticles

The incorporation of QD shells onto the core SPIO NPs was achieved using an electrostatic assembly approach.[32] PEI (50 µL of 10 mg/mL in 0.15 M NaCl, pH 5) was added dropwise into a solution of SPIO-DX NPs (0.5 mL of 1 mg/mL in 0.15 NaCl, pH 5) under vigorous stirring for 20 min. Then, SPIO-DX-PEI NPs were washed (3x) with 0.15 M NaCl to remove unreacted materials using centrifugation (Microcon, YM-100, a cut-off of 100,000 at 10,000 rpm). The collected product was reconstituted in water and added into a solution of QDs in water (1.0 mL, 1.0 mM, pH 9) with vigorous stirring for 20 min. The SPIO-DX-PEI-QDs product was purified and collected by microcentrifuge procedure described above and finally redispersed in water.

The final coating process was achieved by adding PEI solution (70 µL, 10 mg/mL) into a solution of SPIO-DX-PEI -QDs and stirring for 20 min. The final hybrid NPs were collected, washed and redispersed in PBS buffer at pH 7.4.

For the modified electrostatic assembly approach, PEI stabilized AIS/ZnS QDs or SPIO NPs were used for further assembly. Briefly, AIS/ZnS-PEI QDs (0.1 mL) was added into a solution of SPIO-DX NPs (0.5 mg/mL) and the mixture was stirred for 20 min. The final product was separated from the unreacted precursors using the magnetic concentrator and washed with water (3×).

In the case of PEI-stabilized SPIO NPs, AIS/ZnS-GSH QDs (60 µL) were added into a stirring solution of SPIO-PEI NPs (0.05 mmol in 0.5 mL water). After 20 min, the unbound QDs were separated using the magnetic concentrator.

Fabrication of the hybrid probe from QDs and SPIO NPs was achieved using formed silica NPs as a host matrix.

Toward that approach, SPIO NPs can be directly incorporated into a formed silica shell by using the reversed microemulsion approach.[33,34] Typically, a combination of IGEPAL (1.3 mL), SPIO NPs (25 µL) in chloroform, TEOS (120 µL) and ammonia aqueous solution (100 µL, 29 wt.%) was sequentially added to cyclohexane (10 mL) at 15 min intervals under vigorous stirring at room temperature. After 24h of stirring the formed particles were washed by ethanol (3×).

The surface of silica NPs with incorporated SPIO NPs was coated with PEI or MPTMS or GOPTS. For the surface coating with PEI,[35] a solution of SPIO-SiO_2 NPs in ethanol (0.2 mL) was added to ethanolated PEI solution (5 mg/mL) with vigorous stirring. After 1 hr, PEI-coated NPs were precipitated by centrifugation (14,500 rpm, 10 min) and washed (3×) to remove unreacted materials. The silica surface functionalization by mercapto and epoxy groups was achieved by heating the magnetic silica in 1% toluene solution of silane for 1h.[36] Finally, the products were washed with toluene and ethanol (3×, each).

QDs stabilized by GSH were attached to the PEI functionalized silica through electrostatic interactions. In this work, a solution of QDs in water (0.05 mL) was added to SPIO-SiO_2-PEI NPs (0.05 mL) and the reaction vial was stirred for 1h at room temperature. At the end of the reaction, unbound QDs were removed either by centrifugation (4500 rpm for 10 min) or by placing into a magnetic concentrator. The surface coating of the probe with PEI was performed in the same manner as described above. The CIS/ZnS QDs stabilized by amphiphilic polymer were deposited on the surface of SPIO-SiO_2-PEI NPs using the same procedure.

QDs stabilized by GSH were attached to the epoxy groups on the functionalized silica surface through covalent bonds. In brief, the QDs solution (60 µL) was added while stirring to a solution of SPIO-SiO_2-Epoxy NPs (0.5 mL), and 24h later the unbound QDs were removed from the solution by using a magnetic concentrator.

QDs stabilized by OLA were attached to the mercapto functionalized silica surface through covalent linking. OLA-stabilized QDs (20 µL) were added while stirring into a chloroform solution of SPIO-SiO_2-MPTMS (0.5 mL). 24 hrs later, the product was washed thoroughly (3x) on the magnetic concentrator to remove unreacted materials.

The folic acid (FA) conjugation to PEI was achieved using water-soluble coupling reagent, ethyl dimethylaminopropyl carbodiimide (EDC).[36] Briefly, a solution of EDC in PBS (10 mg in 0.2 mL) was added dropwise to a stirring mixture of FA (5.0 mg in 5.0 mL) and PEI (10 mg in 1.0 mL) in PBS (pH 7.4) and the reaction continued for 24h at room temperature. The unreacted FA was removed by centrifugation (3×) (Amicron 3K) and the PEI-FA conjugate was redissolved in PBS. The conjugation percentage of FA to PEI was 30% on a mass ratio basis. It was extrapolated from a calibration curve using known concentrations of FA with an absorption measurement at 285 nm based on a molar extinction coefficient ε=27,500 M^{-1} cm^{-1}. The ATR-FTIR (Bruker Tensor 27) measurements of PEI and PEI-FA conjugate revealed the successful conjugation of folic acid by observation of the 1605 cm^{-1} peak characteristic of an aromatic C=C bond for the FA. The C=O carbonyl peak at 1693 cm^{-1} is diminished due to the conjugation with NH_2- groups of branched PEI.

Characterization

Transmision electron microscopy (TEM) images were obtained via a Philips CM20 and FEI Tecnai Osiris TEM operating at 200 kV. In a typical procedure, a drop of NPs was applied onto an ultrathin-carbon film coated with copper grids (Ted Pella) before observation. A Zetasizer Nano ZS (Malvern Instruments, UK) was used to characterize the hydrodynamic diameter (HD) and zeta potential of NPs. A Cary 5000 UV-vis-NIR spectrometer (Varian) and a Fluorolog-3 FL3-111 (Jobin Yvon/Horiba) were used to measure the absorption and photoluminescence spectra of solutions of NPs at room temperature. The processing and analysis of the captured images was effected using ImageJ (NIH, Wayne Rasband) software.

Results and Discussion

The core-shell assembly approach was used for the fabrication of the MOHNPs (Figure 1). The layered structure had a core of SPIO NPs and a shell assembled from semiconductor QDs. To assemble the QDs onto larger size SPIO NPs, dextran, polyethyleneimine (PEI) or SiO_2 were used. Mercapto and epoxy silanes were also used for the same purpose. PEI was used as a final layer since it stabilizes the system and can provide a transfection capability if used as a delivery agent[37,38] (Figure S1). The fluorescent magnetic hybrid NPs were fabricated from Fe_3O_4 NPs and, $AgInS_2$/ZnS, $CuInS_2$ /ZnS QDs. Appropriate semiconductor QDs were selected based on the desired wavelength of fluorescence emission. The SPIO NPs and QDs with mean sizes below 10 nm were synthesized in aqueous and non-aqueous solutions by colloidal routes. TEM investigation showed that the average sizes of the cadmium-free AIS/ZnS and CIS/ZnS QDs were 3.9 nm and 2.7 nm, respectively (Figure 2A and B). The average sizes of magnetic core SPIO NPs coated with dextran and OLA

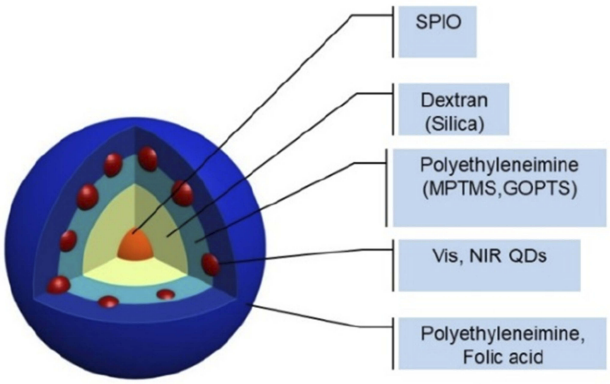

Figure 1 Schematic representation of MOHNPs, which are comprised of SPIO and QDs NPs.

were 5.9 nm and 6.7 nm, respectively (Figure 2C and D). The phase transfer did not significantly alter the particle size or particle size distribution (Figure S2), but provided an additional degree of freedom in particles functionalization. The electrostatic approach used to fabricate the hybrid NPs was based on interactions between oppositely charged assembly components (Figure S1A). For example, as PEI is one of the most successful and widely studied transfection and gene delivery cationic polymers, it was used for encapsulating the semiconductor QDs onto SPIO-DX NPs. During assembly, particle characteristic tracking was done by measurement of the HD (Figure 3A) and zeta potential at different stages of fabrication (Figure 4). As determined by zeta potential measurements, the negative charge of dextran-stabilized SPIO NPs (−8 mV) was used to coat the particles with a layer of positively charged PEI. This coating led to a change in particle charge to 16 mV and a HD diameter enlargement from 28 to 47 nm (Table 1). Consequently, the negatively charged QDs were assembled on the surface of SPIO-DX-PEI NPs. The QDs incorporation was possible based on a strong negative charge possessed by the carboxyl groups of the QD thiol stabilizers. After QD incorporation, the probe charge changed to – 26 mV. The final layer of PEI was assembled on top of the probe for stability and to add cell transfection ability.[38] The HD diameter of the final probe increased to 210 nm, and the charge became positive due to the adsorbed external layer of PEI (30 mV) (Figure 4). The universal applicability of this electrostatic technique allowed the use of QDs possessing negatively charged stabilizers on

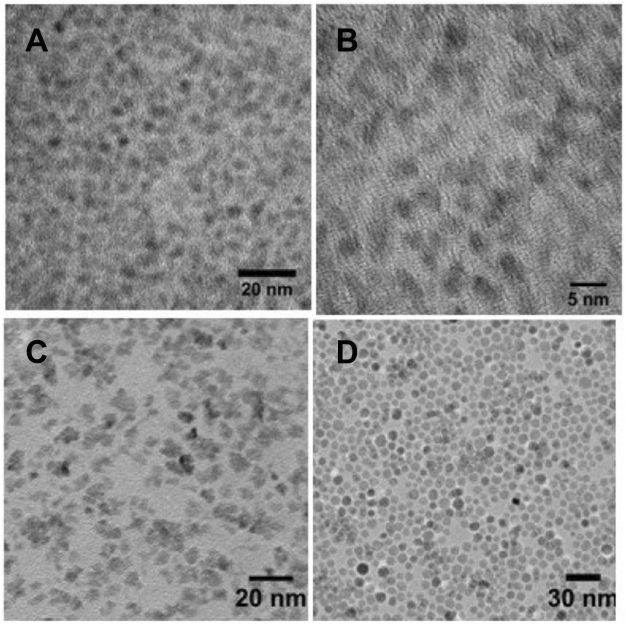

Figure 2 TEM micrographs of synthesized $AgInS_2/ZnS$ (**A**), $CuInS_2/ZnS$ (**B**) QDs and SPIO NPs synthesized in aqueous solution (**C**), oleylamine (**D**).

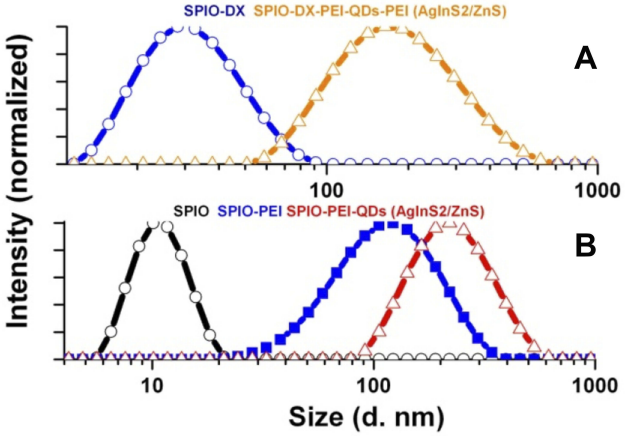

Figure 3 The hydrodynamic diameter of hybrid NPs at different stages of assembly using SPIO NPs synthesized in aqueous solution (**A**), oleylamine (**B**).

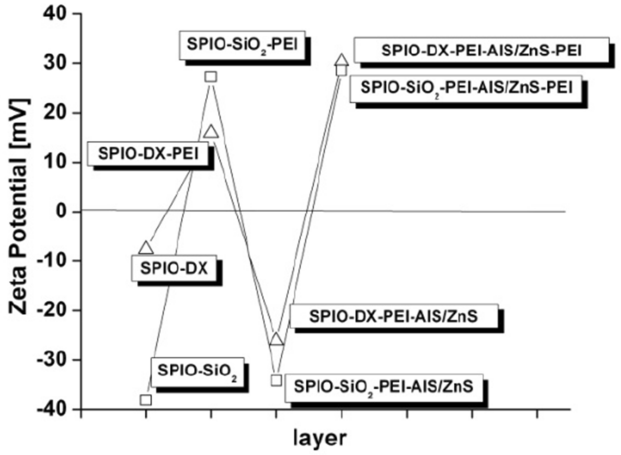

Figure 4 Zeta potential of hybrid NPs at different stages of fabrication.

Table 1 Average Sizes (Z-Average) and Polydispersity Index (PDI) of SPIO Nanoparticles Conjugated to QDs

Sample	d (nm)	PDI
SPIO-DX	27.89	0.15
SPIO-DX-PEI	47.13	0.24
SPIO-DX-PEI-$AgInS_2$/ZnS-PEI	210.4	0.21
SPIO-OLA	16.59	0.10
SPIO-PEI	95.44	0.22
SPIO-PEI-$AgInS_2$/ZnS	208.9	0.16

the surface i.e. glutathione. As a result of these techniques, a wide variety of QDs could be assembled on the surface of SPIO-DX NPs. In this work, by way of illustration, we report the successful assembly of AIS/ZnS QDs.

The same electrostatic assembly procedure was applied to the direct attachment of QDs to PEI-stabilized SPIO NPs (Figure S1B). In this case, SPIO NPs were synthesized in OLA and transferred to the aqueous phase using PEI (Figure S2F). The linking of the PEI layer on the surface of the positively charged magnetic NPs (15 mV) created an excellent electrostatic reception surface for the assembly of negatively charged AIS/ZnS QDs stabilized by GSH. As evidenced by the HD diameter measurements, the expected particle growth was indeed observed (Figure 3B) (Table 1). Moreover, the actual fabrication procedure was also applied for PEI-stabilized QDs when conjugating them with the negatively charged SPIO NPs (Figure S1C).

The aforementioned electrostatic assembly technique was also applied in the attachment of QDs to PEI functionalized SPIO-SiO_2 NPs (Figure S1D). The assembly procedure was checked by measuring the change in surface charge during the deposition steps. The silica surface of SPIO-SiO_2 NPs possessed a negative charge (−38 mV) whereas coating NPs by PEI changed the measured surface charge to a positive value (27 mV). Further, the PEI linking layer enabled the assembly of negatively charged GSH-stabilized AIS/ZnS QDs on the surface of modified SPIO-SiO_2. The hybrid NPs fabrication was completed by the addition of the PEI outer layer. To further illustrate the universality of this electrostatic fabrication approach using SPIO-SiO_2 NPs, CIS/ZnS QDs were also incorporated into hybrid NPs.

In addition to using PEI as a linking layer, silanes with thiol or epoxy functional groups were used for the covalent binding of QDs to the surface of SPIO-SiO_2 NPs (Figure S1D). In the case of thiol silanes, the coating of hybrid NPs with QDs was achieved by linking expressed thiol groups directly to the surface of semiconductor AIS/ZnS QDs stabilized by OLA, based on a ligand exchange mechanism. For epoxy silanes, covalent linkage was achieved through a reaction between the epoxy and amino groups from the SPIO-SiO_2 and the QDs stabilized by GSH, respectively.

Probe construction using SiO_2 interlayer was investigated by TEM microscopy (Figure 5). In the first stage, the formation of highly monodisperse SPIO-SiO_2 core-shell structures was revealed (Figure 5A). As noted above, the control over the distance between the magnetic core and luminescent QDs was achieved by varying the thickness of the SiO_2 shell (Figure S3) such that it would prevent the quenching effect of the iron core on the photoluminescence of the semiconductor QDs but also permit tuning the size of the final composite. The attachment of QDs to the surface of functionalized SPIO-SiO_2 NPs was seen clearly in the TEM images (Figure 5B). As a control, a QDs coating on bare SiO_2 NPs was achieved as well

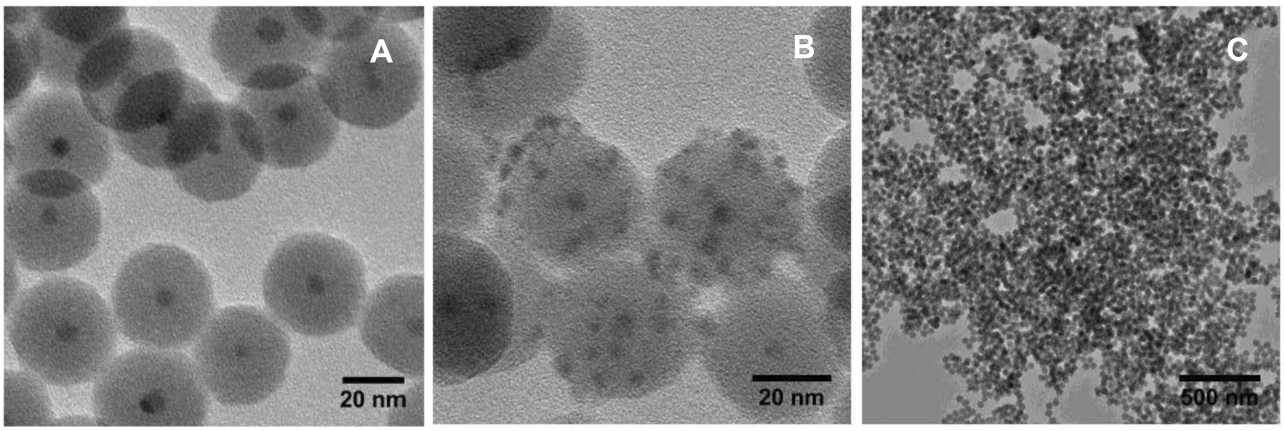

Figure 5 High-resolution TEM images of SPIO NPs incorporated into silica (**A**) and further coated by $AgInS^2$/ZnS QDs (**B**) with low-resolution TEM image (**C**) of a large number of NPs than in (**B**).

(Figure S4). QD binding to the surface of thiol and epoxy silanes functionalized with SiO_2 was also verified by TEM (Figure S5). The structure of fabricated hybrid NPs consisting of SPIO and ZAIS/ZnS QDs was also confirmed by energy dispersive X-Ray spectroscopy (EDS) elemental and high-angle annular dark-field (HAADF) analysis (Figure S6).

The magnetic nature of these synthesized hybrid nanocomposites allowed the particles to be magnetically separated by decantation. The formed composites possess luminescence under UV illumination, which is a further evidence of successful QD conjugation to SPIO NPs using the suggested routes (Figure 6). The assembly of differently structured and sized QDs used for composite construction allowed tuning of the emission wavelength of the resulting hybrid probes (Figure 7). More importantly, the emission wavelength was tuned successfully to 800 nm, which is the window of optimum optical transparency for biological tissue (Figure 7A–C).[39] One particular advantage of the

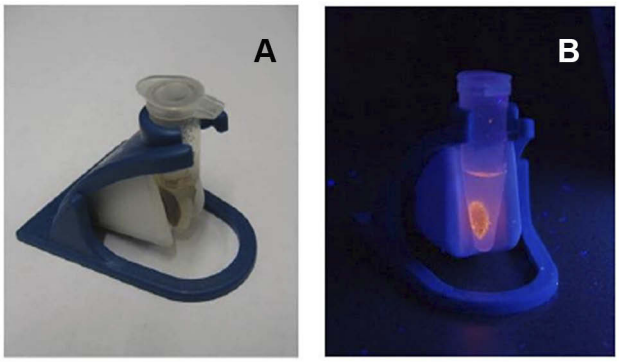

Figure 6 Hybrid NPs placed in magnetic concentrator under ambient light (**A**) and UV-irradiation (**B**).

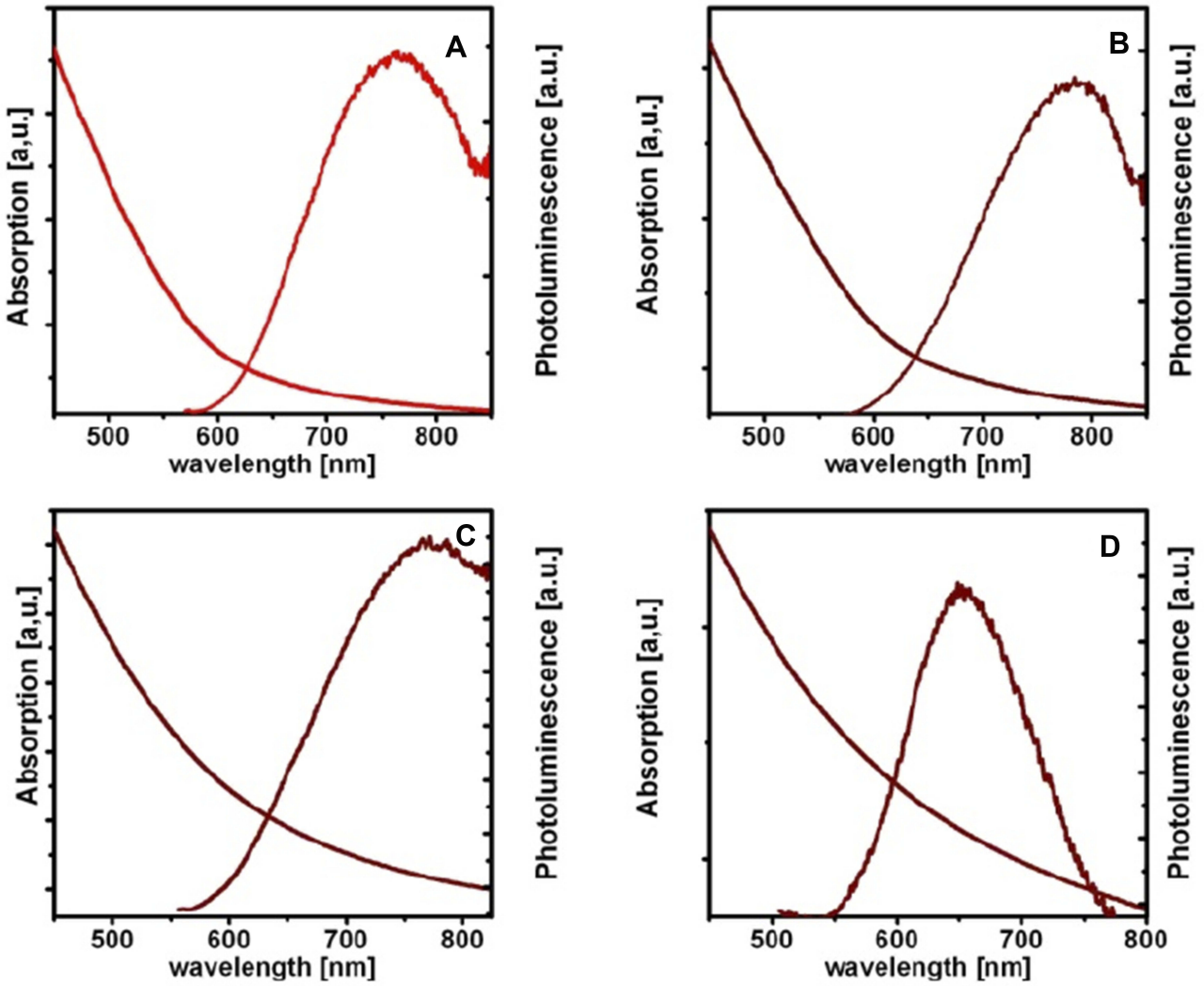

Figure 7 Optical absorption and photoluminescence spectra of differently structured hybrid NPs containing $AgInS_2$/ZnS (**A**–**C**), $CuInS_2$/ZnS (**D**) with the composition SPIO-DX-PEI-QDs-PEI (**A**–**C**), SPIO-PEI-QDs (**D**), SPIO-SiO_2-PEI-QDs-PEI (**C, D**) to allow tuning of the emission wavelength of the resulting hybrid probes.

diverse assembly techniques described in this work is the excellent control that can be exerted over the structure of the composites and the evident ability to tune both the optical and functional properties of the hybrids. It should also be noted that this work describes hybrid NPs construction using a compound that is significantly less toxic, by contrast with QDs that had typically included cadmium in their formulation. Efficient luminescence was observed for the hybrid NPs containing AIS/ZnS (Figure 7A–C) and CIS/ZnS (Figure 7D) QDs. By using luminescent, cadmium-free QDs in the fabrication of the hybrid composite, the intrinsic toxicity of hybrid NPs was greatly reduced.[11,40,41]

The biotargeting functionality of hybrid NPs can be further tailored by surface coating with the folate(FA)-PEI conjugate. Since the folate receptor is overexpressed on the surface of many cancer cell lines it can be used for cell-selective targeting.[42,43] The conjugation of FA and PEI was conducted via carbodiimide chemistry and was confirmed by FTIR-ATR analysis (Figure S7). The coating of hybrid NPs by FA-PEI was conducted as a final external coating electrostatic assembly step over the QDs layer, thereby providing the desired targeting capabilities. The luminescence of hybrid NPs remained stable as evidenced by photoluminescence measurements (Figure S8).

Conclusion

In summary, MOHNPs have been fabricated through the assembly of semiconductor QDs and SPIO NPs. The universal character of the assembly techniques permitted the use of a variety of QDs including cadmium-free QDs. The luminescence wavelength of the hybrid nanoparticles was tuned by adjusting the size and structure of the QDs. The emission range of the hybrid probes was extended into the NIR window to facilitate in vivo imaging applications. Furthermore, the surface structure of the hybrid probe was shown to be readily manipulable to permit the implementation of various targeting transfection capabilities. The resulting hybrid nanoparticles may offer widespread application in biomedical imaging as multimodal probes.

Acknowledgements

This work was partially funded by an NIH grants R01CA160700, R01AG061138. The authors acknowledge support from Vanderbilt Institute of Imaging Science and Vanderbilt Institute of Nanoscale Science and Engineering.

Disclosure

The authors report no conflicts of interest in this work.

References

1. Shikha S, Salafi T, Cheng JT, Zhang Y. Versatile design and synthesis of nano-barcodes. *Chem Soc Rev*. 2017;46(22):7054–7093. doi:10.1039/C7CS00271H
2. Wen CY, Xie HY, Zhang ZL, et al. Fluorescent/magnetic micro/nano-spheres based on quantum dots and/or magnetic nanoparticles: preparation, properties, and their applications in cancer studies. *Nanoscale*. 2016;8(25):12406–12429. doi:10.1039/C5NR08534A
3. Bakalova R, Zhelev Z, Aoki I, Kanno I. Designing quantum-dot probes. *Nat Photonics*. 2007;1(9):487–489. doi:10.1038/nphoton.2007.150
4. Louie AY. Multimodality imaging probes: design and challenges. *Chem Rev (Washington, DC, U S)*. 2010;110(5):3146–3195. doi:10.1021/cr9003538
5. Zhang M, Zheng T, Sheng BL, et al. Mn2+ complex-modified polydopamine- and dual emissive carbon dots based nanoparticles for in vitro and in vivo trimodality fluorescent, photothermal, and magnetic resonance imaging. *Chem Eng J (Lausanne)*. 2019;373:1054–1063. doi:10.1016/j.cej.2019.05.107
6. Fedorenko S, Stepanov A, Sibgatullina G, et al. Fluorescent magnetic nanoparticles for modulating the level of intracellular Ca2+ in motoneurons. *Nanoscale*. 2019;11(34):16103–16113. doi:10.1039/C9NR05071J
7. Kim D, Shin K, Kwon SG, Hyeon T. Synthesis and biomedical applications of multifunctional nanoparticles. *Adv Mater (Weinheim, Ger)*. 2018;30(49). doi:10.1002/adma.201802309
8. He SL, Zhang HW, Delikanli S, Qin YL, Swihart MT, Zeng H. Bifunctional magneto-optical FePt-CdS hybrid nanoparticles. *J Phys Chem C*. 2009;113(1):87–90. doi:10.1021/jp806247f
9. Smith AM, Ruan G, Rhyner MN, Nie S. Engineering luminescent quantum dots for in vivo molecular and cellular imaging. *Ann Biomed Eng*. 2006;34(1):3–14. doi:10.1007/s10439-005-9000-9
10. Bruchez M Jr., Moronne M, Gin P, Weiss S, Alivisatos AP. Semiconductor nanocrystals as fluorescent biological labels. *Science (Washington, DC)*. 1998;281(5385):2013–2016. doi:10.1126/science.281.5385.2013
11. Wagner AM, Knipe JM, Orive G, Peppas NA. Quantum dots in biomedical applications. *Acta Biomater*. 2019;94:44–63. doi:10.1016/j.actbio.2019.05.022
12. Figuerola A, Di Corato R, Manna L, Pellegrino T. From iron oxide nanoparticles towards advanced iron-based inorganic materials designed for biomedical applications. *Pharmacol Res*. 2010;62(2):126–143. doi:10.1016/j.phrs.2009.12.012
13. Veiseh O, Gunn JW, Zhang MQ. Design and fabrication of magnetic nanoparticles for targeted drug delivery and imaging. *Adv Drug Delivery Rev*. 2010;62(3):284–304. doi:10.1016/j.addr.2009.11.002
14. Palanisamy S, Wang YM. Superparamagnetic iron oxide nanoparticulate system: synthesis, targeting, drug delivery and therapy in cancer. *Dalton Trans*. 2019;48(26):9490–9515. doi:10.1039/C9DT00459A
15. Corr SA, Rakovich YP, Gun'ko YK. Multifunctional magnetic-fluorescent nanocomposites for biomedical applications. *Nanoscale Res Lett*. 2008;3(3):87–104. doi:10.1007/s11671-008-9122-8
16. Koole R, Mulder WJM, van Schooneveld MM, Strijkers GJ, Meijerink A, Nicolay K. Magnetic quantum dots for multimodal imaging. *Wiley Interdiscip Rev Nanomed Nanobiotechnol*. 2009;1(5):475–491. doi:10.1002/wnan.14
17. Quarta A, Di Corato R, Manna L, Ragusa A, Pellegrino T. Fluorescent-magnetic hybrid nanostructures: preparation, properties, and applications in biology. *IEEE T Nanobiosci*. 2007;6(4):298–308. doi:10.1109/TNB.2007.908989
18. De Jong WH, Borm PJA. Drug delivery and nanoparticles: applications and hazards. *Int J Nanomedicine*. 2008;3(2):133–149. doi:10.2147/IJN.S596
19. Zhang Q, Li HQ, Ma Y, Zhai TY. ZnSe nanostructures: synthesis, properties and applications. *Prog Mater Sci*. 2016;83:472–535. doi:10.1016/j.pmatsci.2016.07.005

20. Reiss P, Carriere M, Lincheneau C, Vaure L, Tamang S. Synthesis of semiconductor nanocrystals, focusing on nontoxic and earth-abundant materials. *Chem Rev (Washington, DC, U S)*. 2016;116(18):10731–10819. doi:10.1021/acs.chemrev.6b00116
21. Torimoto T, Adachi T, Okazaki K, et al. Facile synthesis of ZnS-AgInS2 solid solution nanoparticles for a color-adjustable luminophore. *J Am Chem Soc*. 2007;129(41):12388–12389. doi:10.1021/ja0750470
22. Torimoto T, Ogawa S, Adachi T, et al. Remarkable photoluminescence enhancement of ZnS-AgInS2 solid solution nanoparticles by post-synthesis treatment. *Chem Commun (Cambridge, U K)*. 2010;46(12):2082–2084. doi:10.1039/b924186h
23. Pong BK, Trout BL, Lee JY. Modified ligand-exchange for efficient solubilization of CdSe/ZnS quantum dots in water: a procedure guided by computational studies. *Langmuir*. 2008;24(10):5270–5276. doi:10.1021/la703431j
24. Zhong XH, Zhang WJ, Chen GJ, Wang J, Ye BC. Design and synthesis of highly luminescent near-infrared-emitting water-soluble CdTe/CdSe/ZnS core/shell/shell quantum dots. *Inorg Chem*. 2009;48(20):9723–9731. doi:10.1021/ic9010949
25. Koktysh D, Bright V, Pham W. Fluorescent magnetic hybrid nanoprobe for multimodal bioimaging. *Nanotechnology*. 2011;22(27):275606. doi:10.1088/0957-4484/22/27/275606
26. Duan HW, Nie SM. Cell-penetrating quantum dots based on multivalent and endosome-disrupting surface coatings. *J Am Chem Soc*. 2007;129(11):3333–3338. doi:10.1021/ja068158s
27. Park J, Kim SW. CuInS2/ZnS core/shell quantum dots by cation exchange and their blue-shifted photoluminescence. *J Mater Chem*. 2011;21(11):3745–3750. doi:10.1039/c0jm03194a
28. Lin CAJ, Sperling RA, Li JK, et al. Design of an amphiphilic polymer for nanoparticle coating and functionalization. *Small*. 2008;4(3):334–341. doi:10.1002/smll.200700654
29. Woo K, Hong J. Surface modification of hydrophobic iron oxide nanoparticles for clinical applications. *IEEE Trans Magn*. 2005;41(10):4137–4139. doi:10.1109/TMAG.2005.855343
30. Mowat P, Franconi F, Chapon C, et al. Evaluating SPIO-labelled cell MR efficiency by three-dimensional quantitative T-2* MRI. *NMR Biomed*. 2007;20(1):21–27. doi:10.1002/(ISSN)1099-1492
31. Xu ZC, Shen CM, Hou YL, Gao HJ, Sun SS. Oleylamine as both reducing agent and stabilizer in a facile synthesis of magnetite nanoparticles. *Chem Mater*. 2009;21(9):1778–1780. doi:10.1021/cm802978z
32. Mackay PS, Kremers GJ, Kobukai S, et al. Multimodal imaging of dendritic cells using a novel hybrid magneto-optical nanoprobe. *Nanomed-Nanotechnol*. 2011;7(4):489–496. doi:10.1016/j.nano.2010.12.004
33. Darbandi M, Thomann R, Nann T. Single quantum dots in silica spheres by microemulsion synthesis. *Chem Mater*. 2005;17(23):5720–5725. doi:10.1021/cm051467h
34. Zhang BB, Chen BD, Wang YL, Guo FF, Li ZQ, Shi DL. Preparation of highly fluorescent magnetic nanoparticles for analytes-enrichment and subsequent biodetection. *J Colloid Interface Sci*. 2011;353(2):426–432. doi:10.1016/j.jcis.2010.09.084
35. Xia TA, Kovochich M, Liong M, et al. Polyethyleneimine coating enhances the cellular uptake of mesoporous silica nanoparticles and allows safe delivery of siRNA and DNA constructs. *ACS Nano*. 2009;3(10):3273–3286. doi:10.1021/nn900918w
36. Hermanson GT. *Bioconjugate Techniques*. 3rd ed. San Diego, CA: Academic Press; 2013.
37. Furgeson DY, Kim SW. Recent advances in poly(ethyleneimine) gene carrier design. *Acs Sym Ser*. 2006;923:182–197.
38. Li L, He ZY, Wei XW, Wei YQ. Recent advances of biomaterials in biotherapy. *Regen Biomater*. 2016;3(2):99–105. doi:10.1093/rb/rbw007
39. Chinnathambi S, Shirahata N. Recent advances on fluorescent biomarkers of near-infrared quantum dots for in vitro and in vivo imaging. *Sci Technol Adv Mater*. 2019;20(1):337–355. doi:10.1080/14686996.2019.1590731
40. Wang LL, Zheng HZ, Long YJ, et al. Rapid determination of the toxicity of quantum dots with luminous bacteria. *J Hazard Mater*. 2010;177(1–3):1134–1137. doi:10.1016/j.jhazmat.2009.12.001
41. Pons T, Pic E, Lequeux N, et al. Cadmium-free CuInS2/ZnS quantum dots for sentinel lymph node imaging with reduced toxicity. *ACS Nano*. 2010;4(5):2531–2538. doi:10.1021/nn901421v
42. Sudimack J, Lee RJ. Targeted drug delivery via the folate receptor. *Adv Drug Delivery Rev*. 2000;41(2):147–162. doi:10.1016/S0169-409X(99)00062-9
43. Fernandez M, Javaid F, Chudasama V. Advances in targeting the folate receptor in the treatment/imaging of cancers. *Chem Sci*. 2018;9(4):790–810. doi:10.1039/C7SC04004K